Sustainable Environment Research

RESEARCH

Open Access

Selective adsorption of gold ion in wastewater with competing cations by novel thiourea-reduced graphene oxide

Yu-Jie Chen[1], Adrienne Chung[1] and Hsing-Cheng Hsi[1,2*]

Abstract

In this study, selective adsorption experiments of Au were carried out using graphene oxide (GO) and thiourea-reduced GO (TU-rGO). Adsorption experiments using Au, Cu, Pb, and Zn were performed with GO and TU-rGO in order to selectively adsorb Au from simulated waste electric and electronic equipment leachate or printed circuit board wastewater. Optimal adsorption conditions were determined, adsorption isotherm models were fitted, and desorption and regeneration experiments were performed. Additionally, GO and TU-rGO were characterized to better understand the material and propose the adsorption and desorption mechanisms for TU-rGO. It was found that TU-rGO could selectively adsorb Au, achieving a high efficiency of 95–99% at initial Au concentrations of 0.1–10 mg L^{-1} with little to no adsorption of Cu, Pb, and Zn. Moreover, the desorption efficiency of Au by ammonium thiosulfate reached 94% with the adsorption efficiency of TU-rGO decreasing from 99 to 78% after five adsorption and desorption cycles. Isotherm adsorption experiments indicated that the Langmuir model better fitted the adsorption of Au than the Freundlich model. This implied that the adsorption process was mainly controlled by monolayer coverage, with a high Au adsorption capacity of approximately 833 mg g^{-1} for TU-rGO.

Keywords Graphene oxide, Thiourea, Thiourea-reduced graphene oxide, Gold recovery technology

1 Introduction

In the era of rapid technology development, humans have a significant demand for electric and electronic equipment (EEE). Yet, amidst the rapidly increasing EEE demand, it has been noted that the life span of EEE is decreasing. According to the Global E-waste Monitor 2020 of the United Nations University report, 53.6 Mt of waste EEE (WEEE) were produced in 2019 and is projected to grow to 74.7 Mt by 2030 [1]. The composition of WEEE generally includes primary base metals, including Fe, Cu, Al, and Pb, and precious metals including Ag, Au, and Pd. Of the base metals, Cu is the most valuable as its economic value is greater than the others in WEEE scrap. WEEE like PC board scrap, mobile phone scrap, PC mainboard scrap, printed circuit boards (PCBs) scrap, and typical electronic device scraps contain large amounts of Au, especially PC mainboard scrap (566 g t^{-1}), PCBs scrap (110 g t^{-1}), and typical electronic device scrap (1000 g t^{-1}) [2]. Au in WEEE is transferred into the solution via a leaching process. The techniques for the recovery of Au can be divided into three major approaches: mechanical separation, pyrometallurgy, and hydrometallurgy. Hydrometallurgical processes transfer metals from WEEE to solution. Traditionally, leaching agents based on mineral acids, cyanide, thiourea, thiosulfate, or halides [3] are used for base metal and precious

*Correspondence:
Hsing-Cheng Hsi
hchsi@ntu.edu.tw
[1] Graduate Institute of Environmental Engineering, National Taiwan University, Taipei 10617, Taiwan
[2] Advanced Research Center for Green Materials Science and Technology, National Taiwan University, Taipei 10617, Taiwan

metal leaching due to their high-efficiency recovery via a simple procedure [4]. The leaching solution must be further treated for purification and metal recovery to obtain Au. Several methods can be used to purify and recover Au from leaching solution, like chemical precipitation, ion exchange by resin, electrodeposition, and adsorption [3, 5]. The drawback of electrodeposition pertains to its non-selectivity. The most common chemical precipitation method is pH adjustment by adding a significant amount of alkali. Thus, due to the recent focus on environmental protection and worker safety, future technologies should prioritize environmental safety [3]. Therefore, adsorption technology for Au recovery from wastewater is most desirable, as it is both environmentally friendly and effective, as adsorbents can be reused and little to no toxic substances are used in this method [6].

Recently, many advancements have been made in the field of Au adsorption. Adsorbents have been derived from several different materials, including metal organic frameworks (MOFs) [7], organic polymers [8], bio-adsorbents [9], biochar and activated carbon [10], and more. To demonstrate, Wang et al. [7] developed a novel S, N-rich MOF, for which a maximum adsorption capacity of 1891 mg g^{-1} could be achieved. Ding et al. [8] synthesized organic polymers which had an adsorption capacity of 862 mg g^{-1}. By producing a functionalized biomass-based adsorbent, Rizki et al. [9] was able to reach an adsorption capacity of 232 mg g^{-1}. Per the literature, N- and S-rich materials are shown to be highly effective in the selective recovery of gold [7, 11, 12]. More specifically, thiourea has been used for material functionalization due to its S- and N-containing functional groups and high selectivity for gold [13, 14]. However, many of the current materials like MOFs or organic polymers require arduous preparation and can be costly to produce. In contrast, bio-adsorbents or activated carbon often have low adsorption capacities, as shown above. Furthermore, many materials suffer from acid instability, inhibiting reuse of the material, and rendering the material less cost-efficient.

Graphene is a flat single layer of carbon atoms compacted into two-dimensional honeycomb lattices and is a fundamental building block for other dimensional graphitic materials. Several methods can be used to synthesize graphene, such as mechanical exfoliation [15], chemical synthesis, and chemical vapor deposition (CVD). The main advantage of CVD lies in its production of high-quality graphene sheets with fewer structural and electronic defects; however, its high cost and limited ability for widespread, large-scale production are its disadvantages [16]. Chemical synthesis is an alternative way to produce graphene from graphite. Graphene oxide (GO) is first synthesized from graphite by oxidants. Then, the graphene oxide is reduced by reducing agents, forming reduced GO (rGO). Synthesis of GO has emerged to offer a precursor in the cost-effective, large-scale production of graphene-based materials [17]. The Hummers' method, relatively safe and less time-consuming [18], has been used for GO synthesis in many studies [19 – 21]. Moreover, GO is hydrophilic in character and abundant in surface oxygen functional groups like carbonyl (C = O), carboxyl (O-C = O), and oxygen single bonds (C-O) [19, 20], rendering it appropriate for heavy metal removal from wastewater by adsorption.

During WEEE recycling, Au and other metals may coexist in the wastewater. Therefore, it is imperative to use a proper adsorbent to selectively recover Au from the wastewater. In this research, GO was first synthesized by the Hummers' method. GO was then modified with thiourea to synthesize thiourea-reduced GO (TU-rGO), as many studies have shown that thiourea can capture Au selectively [3, 17, 21]. TU-rGO was then used to selectively separate Au from wastewater due to the nitrogen and sulfur functional groups and their ability to react with Au to form stable compounds [4].

2 Materials and methods

2.1 Synthesis of GO and TU-rGO

GO was synthesized per Hummers' method [18]. First, 2 g of graphite powder (reagent grade, Acros), 1 g of $NaNO_3$ (99%, Acros), and 46 mL of H_2SO_4 (95–98%, J.T. Baker) were placed in a flask, and the mixture was stirred for 1 min in an ice-water bath. Then, 6 g of $KMnO_4$ (99%, J.T. Baker) was cautiously added while the solution temperature was kept below 20 °C. The mixture was subsequently stirred at 35 °C for 3 h. Afterwards, 92 mL of ultrapure water was added, and the mixture was continuously stirred at 98 °C for 30 min, followed by the addition of 100 mL of ultrapure water and 10 mL of 30% H_2O_2 (30% w/w, Merck) in order to reduce excess potassium permanganate. The solid was washed once with 5% HCl (36.5–38%, J.T. Baker) and eight times with ultrapure water. Last, the graphene oxide samples were centrifuged, filtered, and dried in an oven at 45 °C.

TU-rGO was synthesized by modifying GO with thiourea. 0.8 g thiourea was dissolved in ultrapure water, and the resulting solution was put into the GO colloidal suspension (1 g L^{-1}) with a magnetic stir bar and stirred at 95 °C for 8 h. Afterwards, the TU-rGO solution was washed by ultrapure water and filtered, with the solid ultimately drying at 50 °C for 24 h.

2.2 Physical and chemical analysis of GO and TU-rGO

The C, H, N, S, and O contents of GO and TU-rGO were analyzed by an elemental analyzer (EA, Vario EL cube, Elementar). The crystal phase was identified by X-ray

diffraction (XRD, D2 Phaser, Bruker), scanned continuously from 2θ = 5 to 90°, and the data was registered for the crystalline phase for characteristic peaks. The surface chemical compositions of GO and TU-rGO were measured by X-ray photoelectron spectroscopy (XPS, Scientific ESCALAB 250, VG). The morphology of GO and TU-rGO were visualized by scanning electron microscope (SEM, JSM-6510LV, JEOL) and transmission electron microscopy (TEM; Hitachi H-7100). The zeta potentials of GO and TU-rGO were measured to investigate the surface charge of particles (Malvern Zetasizer Nano analyzer). The adsorbents' specific surface area was determined by using the Brunauer–Emmett–Teller (BET) equation based on N_2 adsorption at 77 K (Micromeritics ASAP 2420 analyzer). Detailed descriptions pertaining to the physical and chemical analysis of GO and TU-rGO can be found in Supplementary Materials.

2.3 Batch adsorption experiments

Batch experiments were carried out with GO and TU-rGO. The artificial wastewater containing Cu, Pb, Zn, and Au were prepared by Cu(II) nitrate, lead nitrate, zinc nitrate, and Au ICP standard. The pH of the aqueous solutions was adjusted with HCl or NaOH of 0.01, 0.1, and 1 M, and GO or TU-rGO was added into 50 mL artificial wastewater. The solution containing GO or TU-rGO was shaken in a temperature-controlled reciprocate shake water bath to determine the influencing parameters, including adsorbent dosage (0.01–0.04 g L^{-1}), pH value (2–10), and contact time (12–120 h) at 150 rpm and 30 °C. The effect of adding Cu (20 or 100 mg L^{-1}), Pb (20 mg L^{-1}), and Zn (20 mg L^{-1}) on selective Au adsorption (0.01, 0.1, 1, and 10 mg L^{-1}) was also tested. After the experiment, the solution was filtered with a 0.45 μm syringe filter, and the filtrate containing Cu, Pb, Zn, and Au was analyzed by inductively coupled plasma optical emission spectrometry (ICP-OES, 700 series, Agilent). The removal efficiencies of Cu, Pb, Zn, and Au were calculated by Eq. (1):

$$\text{Removal efficiency (\%)} = \frac{C_0 - C_t}{C_0} \times 100\% \quad (1)$$

where C_0 (mg L^{-1}) is the initial Cu, Pb, Zn, or Au concentration, C_t (mg L^{-1}) is the residual Cu, Pb, Zn, or Au concentration after adsorption of GO or TU-rGO in solution.

2.4 Batch desorption and regeneration experiments

The TU-rGO after Au adsorption was added to ammonium thiosulfate for the desorption experiment, with the fixed dosage of 0.04 g L^{-1}, shaking speed of 150 rpm, contact time of 24 h, temperature of 30 °C, and pH about 7.4. The Au-containing TU-rGO was prepared by the batch Au adsorption experiment to make the Au content about 250 mg kg^{-1}. The tested concentrations of ammonium thiosulfate were 0.05, 0.1, and 0.2 M. Two-step desorption experiments were then conducted by desorbing the Au-containing TU-rGO to ammonium thiosulfate of 0.05, 0.1, and 0.2 M twice. Based on the aforementioned test results, experiments of repeating adsorption and desorption were also conducted for five times to test the reusability of TU-rGO. Each of filtered solution of Au after adsorption and desorption was also analyzed by ICP-OES.

3 Results and discussion

3.1 Physical and chemical analyses of GO and TU-rGO

Table 1 shows the EA results for GO and TU-rGO. After modification, the oxygen content increased markedly from 0.3% for graphite to 40.0% for GO. The primary contents of GO were 47.2% carbon and 40.0% oxygen. GO was then modified with thiourea to form TU-rGO, in which the amounts of nitrogen and sulfur increased to 2.0 and 22.9%, respectively. Additionally, the oxygen content of GO after modification was reduced from 40.0 to 10.0%.

The crystal phases of graphite, GO, and TU-rGO are shown in Fig. 1. The results indicated that the diffraction peak for graphite was detected at 2θ = 26.5° and the diffraction peak for GO was detected at 2θ = 10.5° [20]. The relatively weaker diffraction peak appearing at 2θ = 23.05° represented the characterization of TU-rGO, corresponding to previous research [22].

Figures 2a and b show the SEM of GO and TU-rGO. The surface micrograph of GO shows a layered graphitic structure and TU-GO depicts a highly folded structure resulting from the doping of sulfur atoms [23]. The TEM images of GO and TU-rGO are shown in Figs. 2c and d. Both GO and TU-rGO presented in multilayer structures, due to which the measured specific surface areas of GO and TU-rGO were only 2.1 and 4.5 m^2 g^{-1} respectively, much less than the theoretical specific surface area of monolayer graphene (i.e., 2630 m^2 g^{-1}) [16]. Additionally, a folded structure was shown on the edge of TU-rGO, which was less significant in GO sheets.

The GO XPS spectra for C1s and O1s are shown in Fig. S1. For the C1s spectrum, four peaks could be deconvoluted from the spectrum. The prominent peaks were the

Table 1 Elemental analysis of graphite, GO, and TU-rGO

	C (%)	O (%)	H (%)	N (%)	S (%)
Graphite	98.6 ± 0.2	0.3 ± 0.0	0.5 ± 0.0	0.2 ± 0.1	0.4 ± 0.1
GO	47.2 ± 0.0	40.0 ± 1.7	2.8 ± 0.1	0.1 ± 0.0	3.7 ± 0.0
TU-rGO	60.4 ± 1.2	10.0 ± 0.1	1.1 ± 0.1	2.0 ± 0.2	22.9 ± 0.3

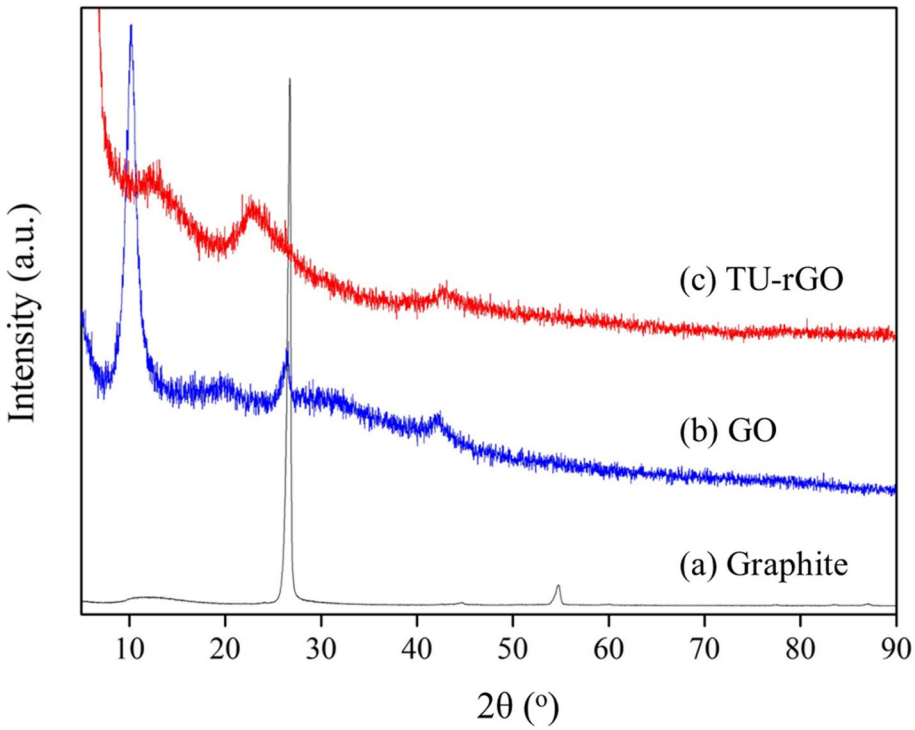

Fig. 1 X-ray diffraction patterns of material (**a**) graphite; (**b**) GO; (**c**) TU-rGO

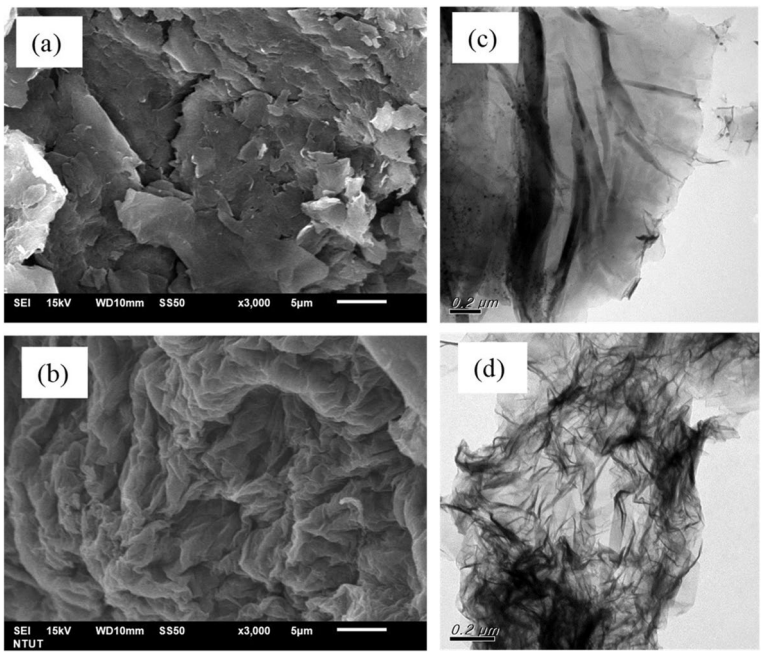

Fig. 2 SEM images of (**a**) GO and (**b**) TU-rGO under 3000 × magnification and TEM image of (**c**) GO and (**d**) TU-rGO under 60,000 × magnification

carbon single bond (C–C) at 284.8 eV, the carbon and oxygen single bond (C-O) at 286.5 eV, carbonyl (C = O) at 285.5 eV, and carboxyl (O-C = O) at 289.1 eV [19]. For the O1s spectrum as well, four peaks were deconvoluted. The main peaks were C-O at 532.9 eV, C = O at 532.1 eV, and O-C = O at 533.6 eV [19, 24]. The TU-rGO XPS

spectra for C1s, O1s, N1s, and S2p are shown in Fig. S2. The intensity of C-O binding energy decreased due to the thiourea modification of GO to form TU-rGO. For the spectrum of O1s for TU-rGO, the areal fraction of C-O binding energy also significantly reduced from 52.1 to 6.7%, proving that the oxygen functional groups on GO were reduced by thiourea. Three peaks could be deconvoluted from the spectrum in the N1s spectrum. The main peaks were pyrrolic-N at 399.8 eV, pyridinic-N at 398.6 eV, and graphite-N at 401.3 eV [3]. For the spectrum of S2p, the main peaks were C-S ($2p_{3/2}$) at 164.1 eV and C-S ($2p_{1/2}$) at 165.2 eV [3, 25].

3.2 Effect of TU-rGO dosage on Au adsorption

The experimental results for TU-rGO dosage are shown in Fig. 3. The removal efficiency of Au reached 83 ± 6% for 0.01 g L^{-1} of TU-rGO dosage due to the complexation of sulfur and nitrogen functional groups with Au [26]. The removal efficiency achieved a plateau of approximately 90% at a dosage greater than 0.02 g L^{-1} TU-rGO for Au. Hence, 0.01 g L^{-1} TU-rGO was selected to discuss the influence of pH and contact time on the Au adsorption with a margin of change to observe.

3.3 Effect of pH for TU-rGO on Au adsorption

Since pH value plays a vital role in aqueous Au adsorption, pH value was evaluated between 2 and 10. The experimental results are shown in Fig. 4. The removal efficiency of Au was 80–85% between pH 2 and 5; however, when pH exceeded 5, the removal efficiency rapidly decreased. Some studies have indicated that the dominant Au species is $AuCl_4^-$ at pH 2 to 5, and the sulfur and nitrogen functional groups can form complexes with Au [26]. When pH surpasses 5, the dominant Au species are $AuCl_3(OH)^-$, $AuCl_2(OH)_2^-$, $AuCl(OH)_3^-$, and $Au(OH)_4$, which result in difficulty in forming complexes these Au species, and the electrostatic repulsion between Au and TU-rGO in solution also contributes to the decreasing adsorption [26, 27]. The dependence of zeta potentials on pH for GO and TU-rGO also supports the results, as the zeta potential remains negative for both GO and TU-rGO at pH 2–10 (Fig. 5). Notably, the zeta potentials of GO were much more negative than those for TU-rGO, which suggests the poor Au adsorption for GO, which will be shown in Sect. 3.5.

3.4 Effect of contact time for TU-rGO on Au adsorption

In order to understand the adsorption kinetics of TU-rGO for Au, different contact times were selected. The experimental data are shown in Fig. 6. The adsorption equilibrium of Au was approximately 96 h, achieving a removal efficiency of 83 ± 6%. The contact time increasing to 120 h caused an insignificant increase in adsorption. The slow adsorption kinetics was associated with the

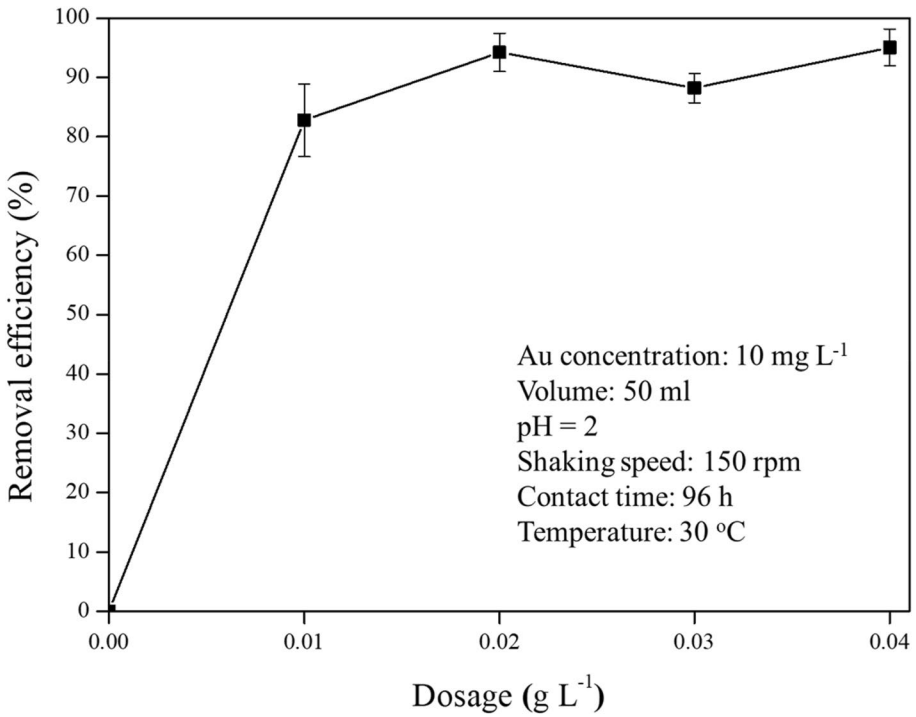

Fig. 3 Effect of adsorbent dosage on Au removal efficiency by TU-rGO

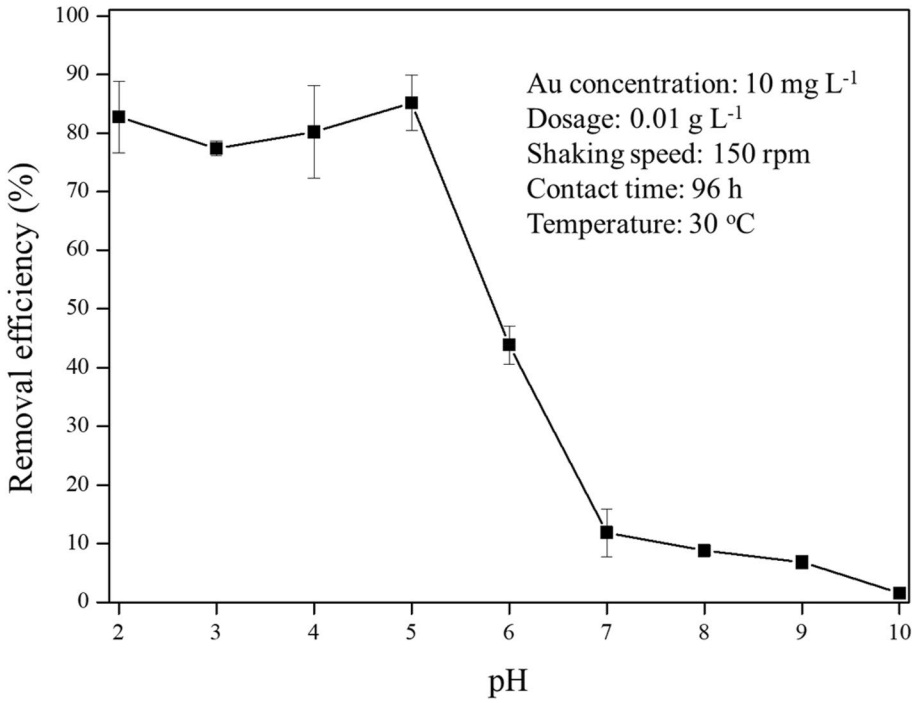

Fig. 4 Effect of pH on Au removal efficiency by TU-rGO

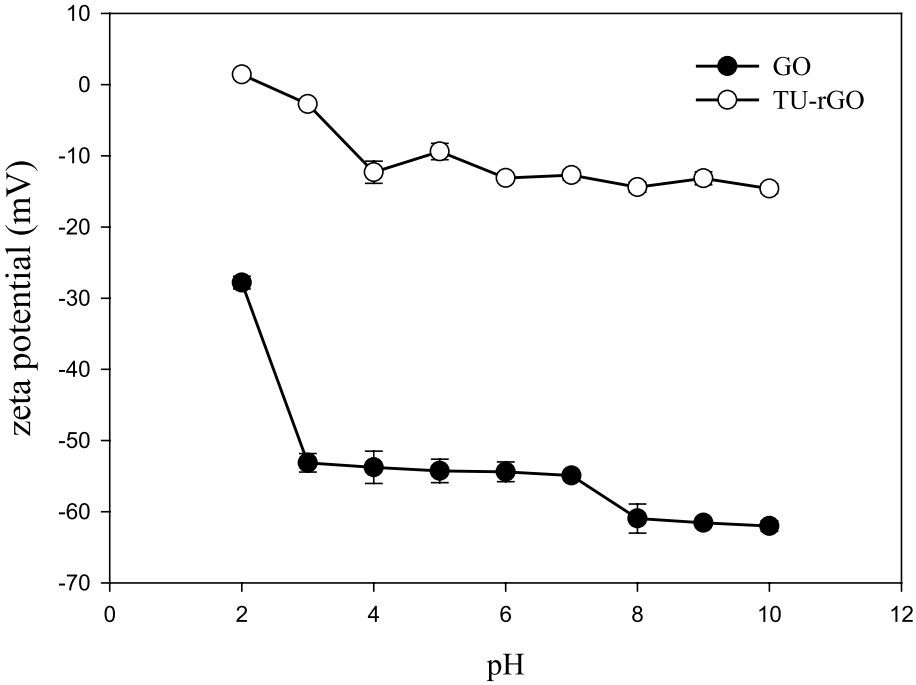

Fig. 5 Zeta potential of GO and TU-rGO as a dependence of pH

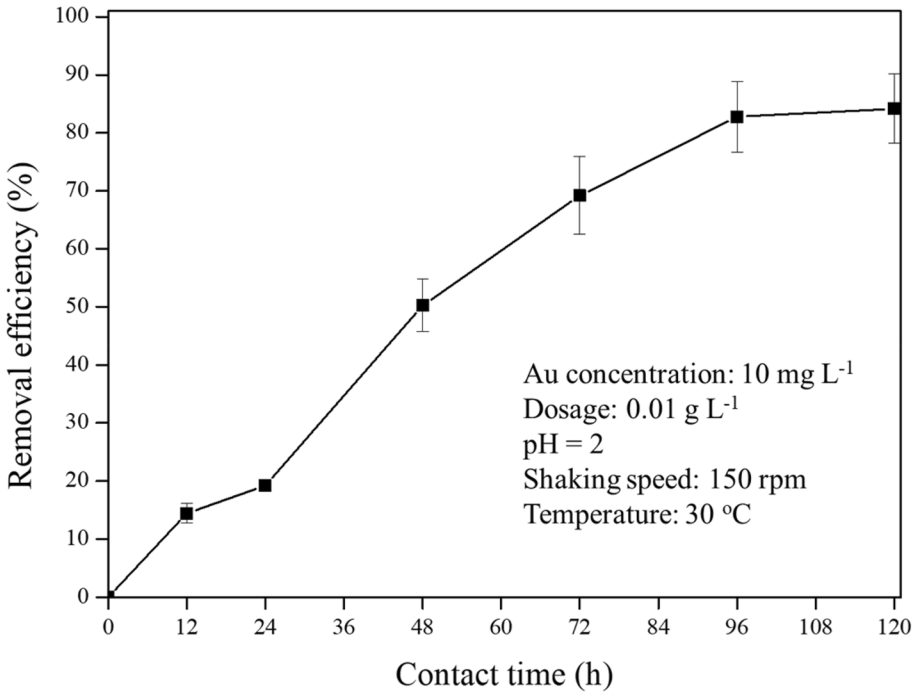

Fig. 6 Effect of contact time on Au removal efficiency by TU-rGO

high activation energy between the sulfur on TU-rGO and Au [28], suggesting chemical reactions between thiourea and Au ions governing the adsorption.

3.5 Selective adsorption experiments of Au with GO and TU-rGO

Figure 7 shows the selective adsorption of TU-rGO at different concentrations of Au and the effect of adding Cu, Pb, and Zn on selective Au adsorption by TU-rGO. As shown in Fig. 7a, the removal efficiency of Au was 98 ± 1% at an initial concentration of 10 mg L^{-1} Au, and Cu, Pb, and Zn were not adsorbed by TU-rGO. Furthermore, when the concentration of Au was decreased to 0.1 mg L^{-1}, the removal efficiency of Au was 99 ± 0% for the selective adsorption experiment. It was demonstrated that the selective adsorption of Au by TU-rGO was not influenced by a differing Au concentration of 10 to 0.1 mg L^{-1}. After the initial Cu concentration was increased to 100 mg L^{-1} as shown in Fig. 7b, the experimental results yielded a lower Au removal efficiency of 95 ± 1% than that obtained at a lower concentration of Cu and an initial Au concentration of 10 mg L^{-1}. When the concentration of Au was decreased to 0.1 mg L^{-1}, the removal efficiency of Au remained at 98 ± 2% by using TU-rGO.

In contrast to Cu and Zn, approximately 1–2% of Pb was adsorbed by TU-rGO due to the presence of oxygen functional groups, as some studies have indicated that the exchange of Pb and hydrogen ions on O-C=O and C-O is responsible for the adsorption of Pb onto GO. The binding energy of Pb with C-O was 5.4 kJ mol^{-1}, and that of Pb with O-C=O was 61.5 kJ mol^{-1}. Therefore, Pb was preferentially bound with O-C=O and was slightly adsorbed by TU-rGO [29, 30].

We also tested the adsorption performance of GO at the same condition; the removal efficiency of Au was only 11 ± 2% (Fig. 8), indicating the importance of thiourea functionality on the TU-rGO surface.

3.6 Desorption experiments of Au-adsorbed TU-rGO

The desorption efficiency of Au is an important factor for Au recovery. In this research, ammonium thiosulfate was used to leach Au from Au-adsorbed TU-rGO. The concentrations of ammonium thiosulfate used were 0.05, 0.1, and 0.2 M; the results are shown in Fig. 9. The greatest desorption efficiency of Au was 94 ± 0% with 0.2 M ammonium thiosulfate. This desorption phenomenon can be explained by the lone electron pairs from nitrogen and sulfur functional groups had on the TU-rGO. According to the Au XPS results, when Au was chemically adsorbed on TU-rGO, it was reduced to elemental Au. The elemental Au collected on the surface of TU-rGO was subsequently oxidized by ammonium thiosulfate to form $Au(S_2O_3)^+$. The reduction potential of thiourea-Au complex is 0.38 V, and that of ammonium thiosulfate with Au is -0.15 V, indicating that ammonium

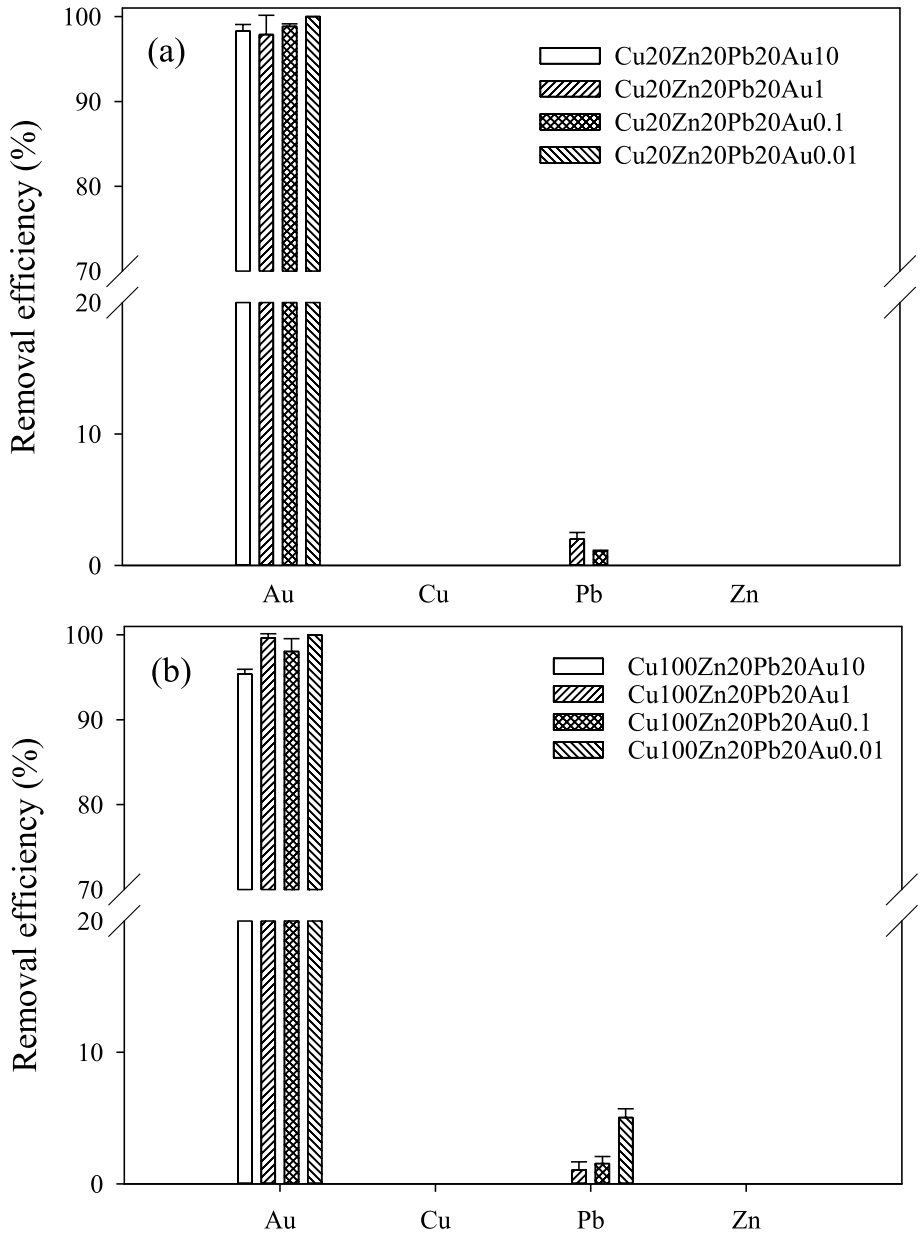

Fig. 7 Selective metal adsorption of TU-rGO at Cu = (**a**) 20 and (**b**) 100 mg L^{-1}. TU-rGO dosage = 0.04 g L^{-1}; shaking speed = 150 rpm; contact time = 96 h; temperature = 30 °C; pH = 2; Pb = 20 mg L^{-1}; Zn = 20 mg L^{-1}; Au = 10, 1, 0.1, 0.01 mg L^{-}.[1]

thiosulfate is a more effective oxidant than thiourea. Therefore, ammonium thiosulfate can be added to form ($Au(S_2O_3)_2^{3-}$), a stable complex, to recover the adsorbed Au from TU-rGO, as opposed to $Au(SC[NH_2]_2)_2^+$, a less stable complex. This can be determined by the respective stability constants of $Au(S_2O_3)_2^{3-}$ ($\log\beta = 26$) and $Au(SC[NH_2]_2)_2^+$ ($\log\beta = 22$) [31].

In order to increase desorption efficiency, a two-step leaching process was tested. Figure 10 depicts the desorption efficiency for the two-step desorption process. A majority of the Au was leached by 0.2 M ammonium thiosulfate during the first step. In the second step, the remaining Au on the TU-rGO surface was leached at three different concentrations of ammonium thiosulfate again. It was found that only an additional 1.4% of Au could be leached by 0.2 M ammonium thiosulfate, demonstrating that two-step leaching was not effective in desorption all of Au on the TU-rGO.

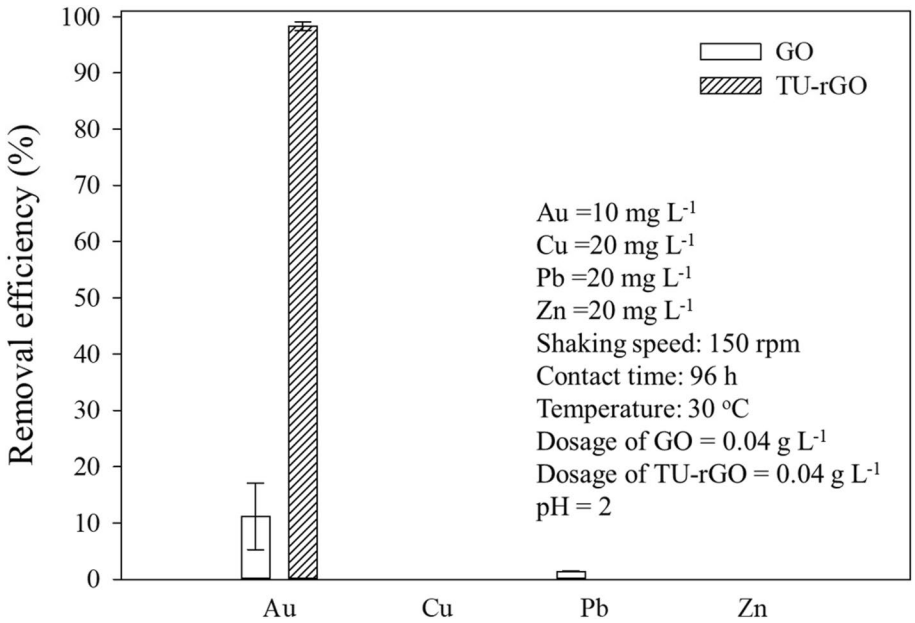

Fig. 8 Comparing with TU-rGO and GO for selective adsorption of Au

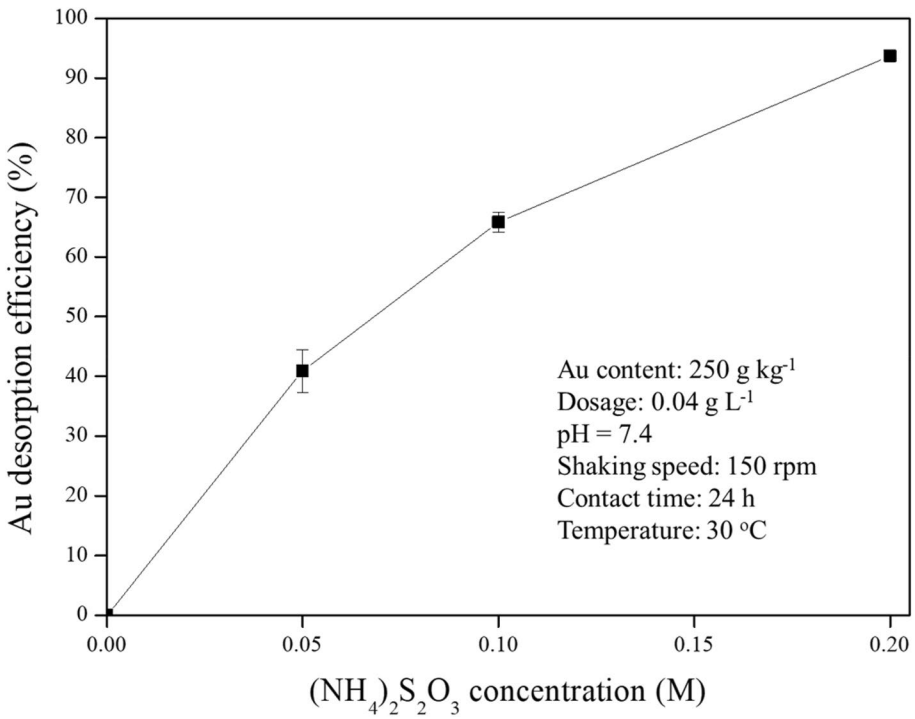

Fig. 9 Effect of ammonium thiosulfate concentration on Au desorption

3.7 Regeneration and reuse experiments of TU-rGO

In order to determine the adsorption efficiency of TU-rGO after multiple cycles of desorption, cycle experiments were carried out by means of five adsorption and desorption sequences. The results are shown in Fig. 11, which revealed that after five cycles, the adsorption efficiency of TU-rGO decreased from 99 ± 1 to 78 ± 1%. This decrease was attributed to the decrease in

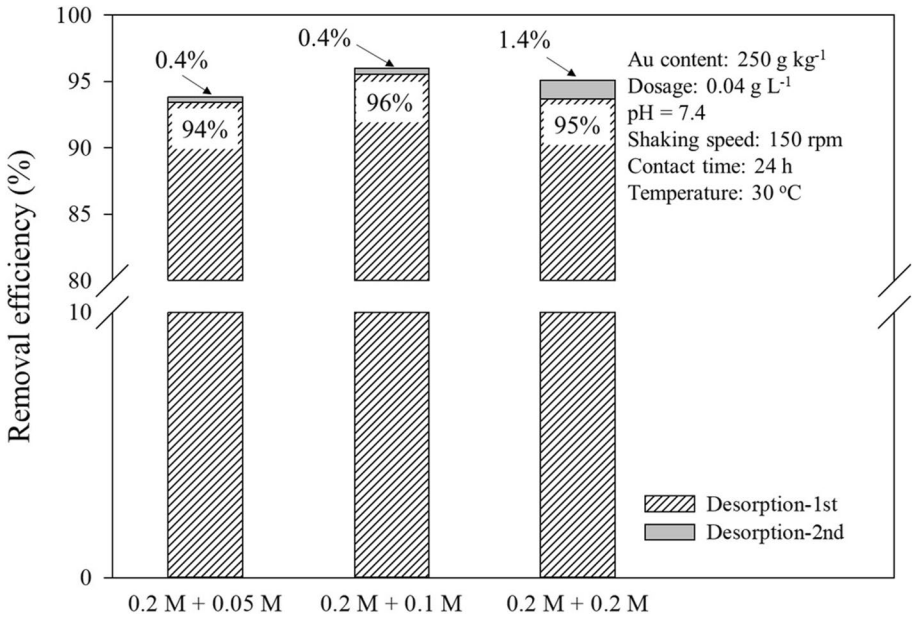

Fig. 10 Two-step desorption of Au from TU-rGO by ammonium thiosulfate

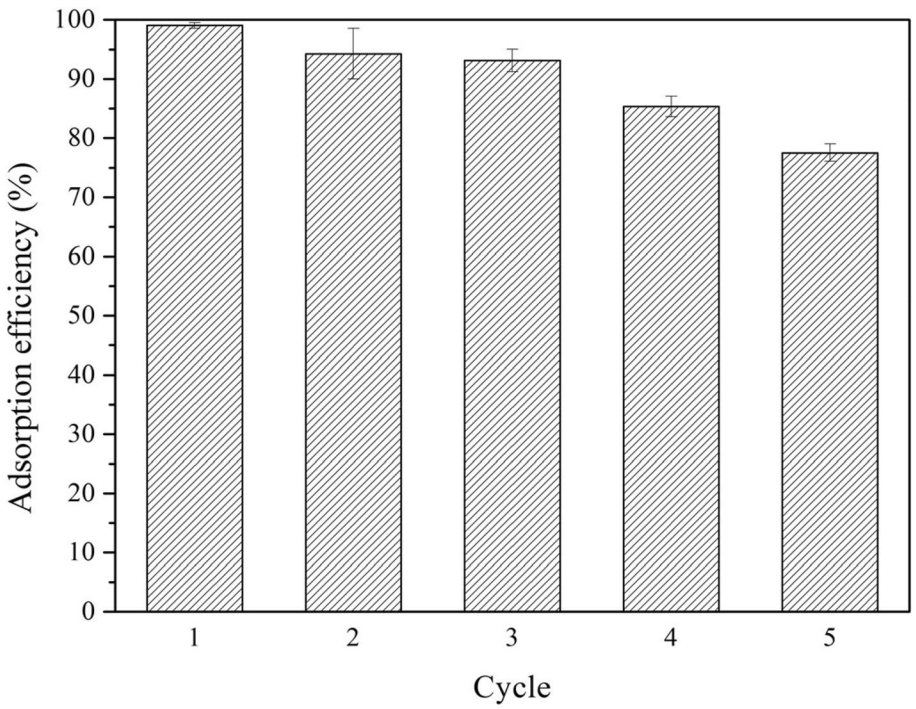

Fig. 11 Adsorption efficiency of TU-rGO in five-cycle experiments (initial Au concentration: 10 mg L^{-1}; TU-rGO dosage: 0.04 g $L^{-.1}$; shaking speed: 150 rpm; contact time: 96 h; temperature: 30 °C; pH: 2)

sulfur functional groups, meanwhile ammonium thiosulfate competed with thiourea for Au. As a result, the bonds between thiourea and TU-rGO were broken by ammonium thiosulfate. This can be inferred from the EA for TU-rGO, such that the amount of sulfur decreased from 23 to 6% after five cycles.

3.8 Au adsorption isotherm experiments and model simulations

Freundlich model and Langmuir model are widely used for the adsorption phenomenon of metals [32]. To determine the fitted isotherms model and parameters, linear forms of isotherm models are widely used. The Freundlich isotherm is represented in Eq. (2). The linear equation of the Freundlich isotherm is described in Eq. (3).

$$q_e = K_F C_e^{1/n} \tag{2}$$

$$\log q_e = \log K_F + \frac{1}{n}\log C_e \tag{3}$$

where q_e is the amount of adsorbate in the adsorbent at equilibrium (mg g^{-1}), K_F is the Freundlich isotherm constant (mg g^{-1}) (L g^{-1}) associated with adsorption capacity, C_e is equilibrium concentration (mg L^{-1}), and n is adsorption intensity.

The Langmuir isotherm model assumes that monolayer adsorption is over a homogeneous adsorbent surface and that no interactions exist between molecules on the surface. The Langmuir isotherm is represented in Eq. (4). The linear equation of Langmuir isotherm is described in Eq. (5).

$$q_e = \frac{Q_0 b C_e}{1 + b C_e} \tag{4}$$

$$\frac{C_e}{q_e} = \frac{1}{bQ_0} + \frac{C_e}{Q_0} \tag{5}$$

where Q_0 is maximum monolayer coverage capacity (mg g^{-1}) and b is Langmuir isotherm constant (L g^{-1}).

The fitted Langmuir and Freundlich models clearly illustrate the relationship between q_e and C_e. The squared correlation coefficients (R^2) and fitting parameters are shown in Table 2. The results indicated that the Langmuir model better fit the adsorption isotherm than the Freundlich model for Au adsorption by TU-rGO, as the squared correlation coefficient (R^2) for Au was 0.915. This suggests that the adsorption process was mainly controlled by monolayer coverage for Au [19]. The q_m value of Au on adsorption of TU-rGO was approximately 833 mg g^{-1}.

Table 2 Langmuir and Freundlich isotherm model for Au adsorption by TU-rGO

Adsorbent	**q_m (mg g^{-1})**	**K_L (L g^{-1})**	**R^2**
TU-rGO	833	11	0.915
Adsorbent	**n**	**K_F (L g^{-1})**	**R^2**
TU-rGO	3.8	293	0.780

3.9 Mechanism of Au adsorption and desorption

A mechanism of Au adsorption and desorption is proposed in this study and is depicted in Fig. 12. The oxygen functional groups present on the GO surface as shown in Fig. 12a, while the thiourea modification process of GO to form TU-rGO is illustrated in Figs. 12b and c. The GO was simultaneously reduced and doped with sulfur and nitrogen. As a result of the highly stable nature of Au with sulfur and nitrogen functional groups, Au was chemically adsorbed on the TU-rGO surface, as given in Fig. 12d. When Au was chemically adsorbed via electrostatic interaction and TU coordination on the TU-rGO, it was reduced [33–36], forming elemental gold from the oxidized sulfur as shown in Fig. 12e. Lastly, ammonium thiosulfate was adopted for the desorption experiments. Elemental Au was oxidized by ammonium thiosulfate and dissolved into aqueous solution. Au generally bound with ammonium thiosulfate amidst competition between ammonium thiosulfate and thiourea for Au. As the reduction potential of thiourea with Au is 0.38 V and the reduction potential of ammonium thiosulfate with Au is -0.15 V, ammonium thiosulfate was a more effective oxidant than thiourea. Therefore, Au combined with thiourea was leached by complexation in the aqueous ammonium thiosulfate solution, as noted in Fig. 12f. As the sulfur functional groups were oxidized and released from TU-rGO, the sulfur content of TU-rGO significantly decreased from 23 to 6% after ammonium thiosulfate treatment.

3.9.1 Comparison of Au adsorption by TU-rGO and other adsorbents

Table 3 illustrates the overall excellent performance of TU-rGO compared to other adsorbents, considering it is able to maintain high recovery efficiency with high Au selectivity at realistically low concentrations found in actual WEEE, which has rarely been studied. Additionally, other adsorbents, similar to those given in Table 3, though having high adsorption capacities, also have high costs or require complicated preparation methods, rendering the material more cost- and time-inefficient than TU-rGO. This further solidifies TU-rGO as an exceptional choice for Au recovery in the future.

4 Conclusions

This study has achieved three major objectives. First, GO was successfully synthesized through Hummers' method and modified with thiourea to develop TU-rGO. The presence of thiourea on TU-rGO was verified through instrumental analysis. Second, the adsorption parameters for Au were investigated to determine the

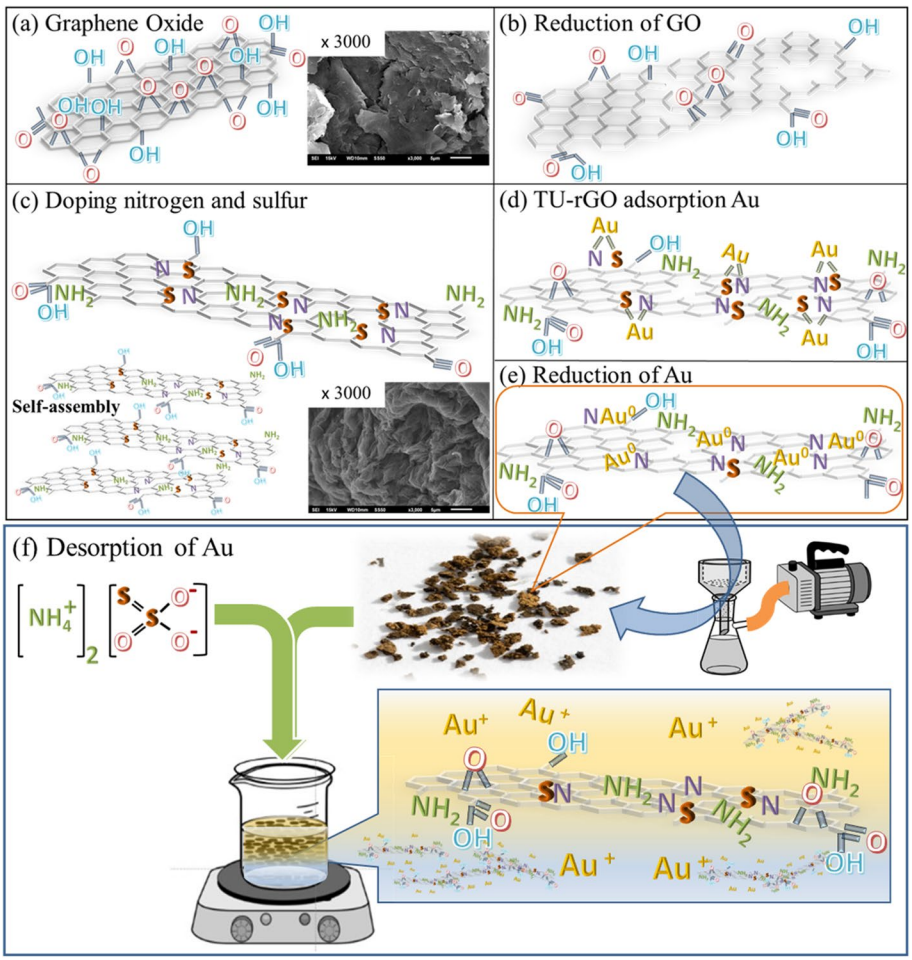

Fig. 12 Mechanism of synthesizing TU-rGO and adsorption and desorption for Au with TU-rGO. **a** synthesis of GO by Hummers' method; **b** reduction of GO; **c** doping of nitrogen and sulfur on the surface of TU-rGO; **d** adsorption of Au by TU-rGO; **e** reduction of Au by the sulfur functional group to form elemental gold on the surface of TU-rGO; **f** desorption of Au from the surface of TU-rGO

optimal adsorption condition; the excellent selectivity of TU-rGO for Au in wastewater was then demonstrated through competitive adsorption experiments. Lastly, the desorption and regeneration efficiency of TU-rGO was found to recover Au from wastewater effectively.

The primary conclusions are summarized as follows. elemental analysis results showed that GO had marked amounts of oxygen, measuring at approximately 40%, owing to the formation of oxygen functional groups. Compared with GO, the nitrogen and sulfur in TU-rGO increased to 2 and 23%, respectively, after thiourea treatment. This is attributed to the nitrogen and sulfur added by substituting oxygen. TU-rGO had excellent selectivity for the adsorption of Au. The optimal parameters for TU-rGO for Au adsorption were 0.01 g L^{-1} for dosage, 96 h of contact time, and pH 2. The recovery of Au achieved 95–98% efficiency at different initial concentrations. For desorption experiments, ammonium thiosulfate was used to compete with thiourea for Au. The thiourea was unstable in an alkaline environment; therefore, Au was effectively desorbed from TU-rGO by ammonium thiosulfate. The desorption efficiency was 94% at 0.2 M ammonium thiosulfate. For regeneration experiments, the adsorption efficiency of TU-rGO decreased from 99 ± 1% to 78 ± 1% after five cycles due to instability and decomposition of thiourea during ammonium thiosulfate treatment. As such, the amount of sulfur decreased from 23 to 6% after five cycles of adsorption and desorption leaching. Lastly, isotherm adsorption experiments suggest that the Langmuir model better fitted the adsorption of Au than the Freundlich model, implying that the adsorption process

Table 3 Au(III) adsorption performance of selected adsorbents

Type/ Adsorbents	Maximum adsorption (mg g^{-1})	Adsorption conditions	Reusability	Adsorption ratio at low concentration	Refs
Organic Polymer: Pc-POSS-POPs	862	pH 3, 35 °C	Reduced from 92 to 91 mg g^{-1} after five cycles	-	[8]
Biomass: SiRH_Im	233	pH 1	No significant decrease after three cycles	-	[9]
Functionalized resin: thiourea@ ZGA451	996	pH 3, 25 °C	Reduced to 92% after five cycles	-	[13]
MOF: DONA-MOF	638	pH 6, 30 °C	Reduced to 89% after five cycles	-	[37]
Core–shell structured magnetic adsorbent: Fe_3O_4@CuS	559	pH 6, room temperature	Reduced to ~ 80% after five cycles	-	[38]
Bio-adsorbent: DAVF-PT	528	pH 2, 25 °C	-	-	[39]
Polymer + GO: HPEI-*g*-PAN/GO-HPEI	2893	pH 4.7, 25 °C	Reduced to 85% after five cycles	-	[40]
Functionalized GO: TU-rGO	833	pH 2, 30 °C	Reduced to 78% after five cycles	95–99% for 0.1–10 mg L^{-1}	This work

was mainly controlled by monolayer coverage, with a high adsorption capacity (about 833 mg g^{-1}) of Au on TU-rGO. The selective recovery and subsequent desorption of Au, as well as the regenerative nature of the material, will allow for the successful recovery of Au from WEEE and wastewater, leading to more successful urban mining in the electric and electronic equipment industry.

Supplementary Information

The online version contains supplementary material available at https://doi.org/10.1186/s42834-024-00227-9.

Supplementary Material 1.

Acknowledgements
The authors wish to thank the supports from the Ministry of Education (112L9006) and the National Science and Technology Council (NSTC 109-2622-E-002-023) of Taiwan. The opinions expressed in this paper are not necessarily those of the sponsor.

Authors' contributions
Conceptualization, H.C.H. and Y.J.C.; methodology, Y.J.C. and H.C.H.; formal analysis, Y.J.C. and A.C.; data curation, Y.J.C. and A.C.; writing—original draft preparation, Y.J.C. and H.C.H.; writing—review and editing, A.C. and H.C.H.; visualization, Y.J.C. and A.C.; funding acquisition, H.C.H. All authors read and approved the final manuscript.

Funding
This study was supported by the Ministry of Education (112L9006) and the National Science and Technology Council (NSTC 109–2622-E-002–023) of Taiwan.

Availability of data and materials
All data generated or analyzed during this study are included in this published article.

Declarations

Competing interests
The authors declare they have no competing interests.

Received: 9 April 2024 Accepted: 13 August 2024
Published online: 20 August 2024

References

1. Forti V, Balde CP, Kuehr R, Bel G. The Global E-Waste Monitor 2020: Quantities, Flows and the Circular Economy Potential. Bonn: United Nations University; Geneva: United Nations Institute for Training and Research, International Telecommunication Union; Rotterdam: International Solid Waste Association; 2020.
2. Zhang L, Xu Z. A review of current progress of recycling technologies for metals from waste electrical and electronic equipment. J Clean Prod. 2016;127:19–36.
3. Li R, Li J, Qi K, Ge X, Zhang Q, Zhang B. One-step synthesis of 3D sulfur/nitrogen dual-doped graphene supported nano silicon as anode for Li-ion batteries. Appl Surf Sci. 2018;433:367–73.
4. Akcil A, Erust C, Gahan CS, Ozgun M, Sahin M, Tuncuk A. Precious metal recovery from waste printed circuit boards using cyanide and non-cyanide lixiviants–a review. Waste Manage. 2015;45:258–71.
5. Lekka M, Masavetas I, Benedetti AV, Moutsatsou A, Fedrizzi L. Gold recovery from waste electrical and electronic equipment by electrodeposition: A feasibility study. Hydrometallurgy. 2015;157:97–106.
6. Liu L, Liu S, Zhang Q, Li C, Bao C, Liu X, et al. Adsorption of Au(III), Pd(II), and Pt(IV) from aqueous solution onto graphene oxide. J Chem Eng Data. 2013;58:209–16.
7. Wang B, Ma Y, Xu W, Tang K. A novel S,N-rich MOF for efficient recovery of Au(III): Performance and mechanism. J Hazard Mater. 2023;451:131051.
8. Ding R, Chen Y, Li Y, Zhu Y, Song C, Zhang X. Highly efficient and selective gold recovery based on hypercross-linking and polyamine-functionalized porous organic polymers. ACS Appl Mater Inter. 2022;14:11803–12.
9. Rizki IN, Amalina I, Hasan NS, Khusnun NF, Jalil AA, Firmansyah ML. Functionalized agriculture-derived biomass-based adsorbent for the

continuous recovery of gold from a simulated mobile phone leachate. Chemosphere. 2023; 345:140455.
10. Zhou W, Liang H, Lu Y, Xu H, Jiao Y. Adsorption of gold from waste mobile phones by biochar and activated carbon in gold iodized solution. Waste Manage. 2021;120: 530–7.
11. Zhang M, Dong Z, Hao F, Xie K, Qi W, Zhai M, et al. Ultrahigh and selective adsorption of Au(III) by rich sulfur and nitrogen-bearing cellulose microspheres and their applications in gold recovery from gold slag leaching solution. Sep Purif Technol. 2021;274:119016.
12. Kantipuly C, Katragadda S, Chow A, Gesser HD. Chelating polymers and related supports for separation and preconcentration of trace metals. Talanta. 1990;37:491–517.
13. Liu C, Song Z, Mao Y, Yan X, Li Z, Liu Y, et al. High selectivity of new thiourea-modified resins for gold: Adsorption performance, mechanism, and recovery. Hydrometallurgy. 2022;213:105944.
14. Ma T, Zhao R, Li Z, Jing X, Faheem M, Song J, et al. Efficient gold recovery from e-waste via a chelate-containing porous aromatic framework. ACS Appl Mater Inter. 2020;2:30474–82.
15. Datta SS, Strachan DR, Khamis SM, Johnson ATC. Crystallographic etching of few-layer graphene. Nano Lett. 2008;8:1912–5.
16. Ghany NAA, Elsherif SA, Handal HT. Revolution of Graphene for different applications: State-of-the-art. Surf Interfaces. 2017;9:93–106.
17. Zhu Y, Murali S, Cai W, Li X, Suk JW, Potts JR, et al. Graphene and graphene oxide: synthesis, properties, and applications. Adv Mater. 2010;22:3906–24.
18. Hummers Jr WS, Offeman RE. Preparation of graphitic oxide. J Am Chem Soc. 1958;80:1339.
19. Sitko R, Turek E, Zawisza B, Malicka E, Talik E, Heimann J, et al. Adsorption of divalent metal ions from aqueous solutions using graphene oxide. Dalton T. 2013;42:5682–9.
20. Chowdhury DR, Singh C, Paul A. Role of graphite precursor and sodium nitrate in graphite oxide synthesis. RSC Adv. 2014; 4:15138–45.
21. Gurung M, Adhikari BB, Kawakita H, Ohto K, Inoue K, Alam S. Recovery of gold and silver from spent mobile phones by means of acidothiourea leaching followed by adsorption using biosorbent prepared from persimmon tannin. Hydrometallurgy. 2013;133:84–93.
22. Satheesh K, Jayavel R. Synthesis and electrochemical properties of reduced graphene oxide via chemical reduction using thiourea as a reducing agent. Mater Lett. 2013;113:5–8.
23. Kannan AG, Zhao J, Jo SG, Kang YS, Kim DW. Nitrogen and sulfur co-doped graphene counter electrodes with synergistically enhanced performance for dye-sensitized solar cells. J Mater Chem A. 2014;2:12232–9.
24. Oh YJ, Yoo JJ, Kim YI, Yoon JK, Yoon HN, Kim JH, et al. Oxygen functional groups and electrochemical capacitive behavior of incompletely reduced graphene oxides as a thin-film electrode of supercapacitor. Electrochim Acta. 2014;116:118–28.
25. Lee WSV, Leng M, Li M, Huang XL, Xue JM. Sulphur-functionalized graphene towards high performance supercapacitor. Nano Energy 2015;12:250–7.
26. Lin G, Wang S, Zhang L, Hu T, Peng J, Cheng S, et al. Synthesis and evaluation of thiosemicarbazide functionalized corn bract for selective and efficient adsorption of Au(III) from aqueous solutions. J Mol Liq. 2018;258:235–43.
27. Garcia-Soto MJ, Gonzalez-Ortega O. Synthesis of silica-core gold nanoshells and some modifications/variations. Gold Bull. 2016;49:111–31.
28. Lowell S, Shields JE, Thomas MA, Thommes M. Characterization of Porous Solids and Powders: Surface Area, Pore Size and Density. Dordrecht: Springer. 2004.
29. Wang X, Chen Z, Yang S. Application of graphene oxides for the removal of Pb(II) ions from aqueous solutions: Experimental and DFT calculation. J Mol Liq. 2015;211:957–64.
30. Peng W, Li H, Liu Y, Song S. A review on heavy metal ions adsorption from water by graphene oxide and its composites. J Mol Liq. 2017;230:496–504.
31. Stofkova M, Stofko M. Ion exchange resin use for Au and Ag separation form diluted solutions of thiourea. Metallurgy. 2002;41:33–6.
32. Sherlala AIA, Raman AAA, Bello MM, Asghar A. A review of the applications of organo-functionalized magnetic graphene oxide nanocomposites for heavy metal adsorption. Chemosphere. 2018;193:1004–17.
33. Lustemberg PG, Vericat C, Benitez GA, Vela ME, Tognalli N, Fainstein A, et al. Spontaneously formed sulfur adlayers on gold in electrolyte solutions: Adsorbed sulfur or gold sulfide? J Phys Chem C. 2008;112:11394–402.
34. Pensa E, Cortes E, Corthey G, Carro P, Vericat C, Fonticelli MH, et al. The chemistry of the sulfur–gold interface: In search of a unified model. Accounts Chem Res. 2012;45:1183–92.
35. Huergo MA, Giovanetti L, Moreno MS, Maier CM, Requejo FG, Salvarezza RC, et al. New insight into the chemical nature of the plasmonic nanostructures synthesized by the reduction of Au(III) with sulfide species. Langmuir. 2017;33:6785–93.
36. Carro P, Andreasen G, Vericat C, Vela ME, Salvarezza RC. New aspects of the surface chemistry of sulfur on Au(III): Surface structures formed by gold-sulfur complexes. Appl Surf Sci. 2019;487:848–56.
37. Chen Y, Tang J, Wang S, Zhang L. Facile preparation of a remarkable MOF adsorbent for Au(III) selective separation from wastewater: Adsorption, regeneration and mechanism. J Mol Liq. 2022;349:118137.
38. Xia J, Ghahreman A. Core–shell structured Fe_3O_4@CuS for effective gold capture and recovery. ACS Appl Nano Mater. 2023;6:10837–44.
39. Liu J, Jin C, Wang C. Hyperbranched thiourea-grafted electrospun polyacrylonitrile fibers for efficient and selective gold recovery. J Colloid Interf Sci. 2020;561:449–58.
40. Li XH, Yang HJ, Ma YX, Li TZ, Meng WL, Zhong XM. A novel PAN/GO electrospun nanocomposite fibrous membranes with rich amino groups for highly efficient adsorption of Au(III). Diam Relat Mater. 2023;137:110175.

Publisher's Note